CHEMISTRY
A EUROPEAN JOURNAL

DOI: 10.1002/chem.200800363

Nucleation and Growth of BaF_xCl_{2-x} Nanorods

Ting Xie, Shuai Li, Wenbei Wang, Qing Peng, and Yadong Li*[a]

Abstract: Different ratios and sizes of Ba_2F_3Cl (BaF_xCl_{2-x}, $x=1.5$) nanorods and nanowires and orthorhombic BaF_2 (BaF_xCl_{2-x}, $x=2$) nanorods were prepared by using a liquid–solid–solution approach at 160~180 °C. The processes and results of the experiments conducted to prepare monodisperse Ba_2F_3Cl nanorods and nanowires showed that the specific surface area increased as the initial concentrations were multiplied. Based on this fact, a mechanism for the nucleation and growth processes of these nanocrystals that have a variety of enlarged sizes was substantiated in view of the surface chemical thermodynamics (SCT). In this SCT mechanism, the specific surface energy takes into account both the surfactant oleic acid and the nanocrystal surface, and is dominated by the chemical potential of the adsorbate.

Keywords: growth mechanism · monodisperse structures · nanostructures · surface chemistry · thermodynamics

Introduction

An understanding the mechanism for the nucleation and growth of nanocrystals has become more and more important recently[1,2] because not only does it provide a variety of monodisperse shapes and sizes of building blocks for nanotechnology,[3–6] it also helps us to develop improved synthetic methods that are generally applicable to various kinds of materials at this length scale with new properties that, importantly, change with their size.[7–14] Many of the properties of nanomaterials can be significantly attributed to their extremely high specific surface area (SSA), which is a result of unsaturated suspended bonds, exterior disfigurements, crystal defects, catalytically active centers on the surface, and so on.[15] Thus, two key factors controlling the properties of nanomaterials are the size and surface characteristics of the nanoparticles.[16–19] Admittedly, the contention that the size of nanocrystals determines their surface area has been fundamentally accepted; these two factors are interrelated. The nucleation and growth processes of these nanocrystals have been carefully discussed and explained by the Peng group regarding the preparation of semiconductors.[20–22] Research on how to prepare nanocrystals with controllable sizes and shapes have been reported universally.[12,18,19,21–31] However, one of the major challenges in the synthesis of nanomaterials is still to gain a comprehensive understanding of monodisperse nanocrystal nucleation and growth, and furthermore, a general and convenient approach to adjust the SSA and control the total surface area of the nanocrystal units, that is, the average surface/atom ratio (δ) of inorganic nanomaterials. To meet this challenge, the emphasis of this work is based on a mechanism of surface chemical thermodynamics that can explain the relation between the initial concentration of reactants and the average δ value of the final products by a unified and relatively simple synthetic condition alteration. Herein, a great effort was made to substantiate the mechanism with experimental results from a hydrothermal synthesis route and, further, to predict the scale of nanocrystals qualitatively in two other approximate systems.

We chose to study the Ba_2F_3Cl and orthorhombic BaF_2 systems because they are dielectric and have a wide range of potential applications in optoelectronic and microelectronic devices, such as dielectrics, wide-gap insulating layers, insulators, buffer layers, and solid-state ions,[32] and because BaF_2 compounds doped with rare-earth ions have been reported to display unique luminescence properties and can thus be used as scintillators.[33] Several BaF_2 nanocrystals have already been reported by Burlitch et al.,[34] Hu et al.,[35] Shi et al.,[36,37] Xie et al.,[38] and Qin et al.[39] All of these nanocrystals are cubic BaF_2 and have nanocube and nanorod shapes. Thus, there is also a great need to synthesize orthorhombic BaF_2. Moreover, to the best of our knowledge,

[a] T. Xie, S. Li, W. Wang, Dr. Q. Peng, Prof. Y. Li
Department of Chemistry
Tsinghua University
Beijing, 100084 (P. R. China)
Fax: (+86) 10-6278-8765
E-mail: ydli@mail.tsinghua.edu.cn

Supporting information for this article is available on the WWW under http://dx.doi.org/10.1002/chem.200800363.

reports concerning Ba_2F_3Cl nanorods and nanowires are quite rare. Herein, the preparation of these nanocrystals, the sizes of which were guided by the SCT mechanism, was accomplished by using the liquid–solid–solution (LSS) approach.[28]

Results and Discussion

The morphology, size, and crystal-phase purity of the as-prepared nanocrystals are significantly dependent on the reaction conditions, such as temperature, time, and initial concentration of the reactants. For the purpose of tailoring the size and shape of the nanocrystals, several works[40,41] have been completed by our group, in which these synthetic condition parameters were adjusted. When we prepared Ba_2F_3Cl nanorods by using the LSS synthetic strategy, an exciting experimental result indicated that the Ba_2F_3Cl nanorods increased in both length and width as the initial reactant concentration ($[Ba^{2+}]$) was altered from $0.1000\,mol\,L^{-1}$ (Figure 1a) to $0.0750\,mol\,L^{-1}$ (Figure 1b), and finally to

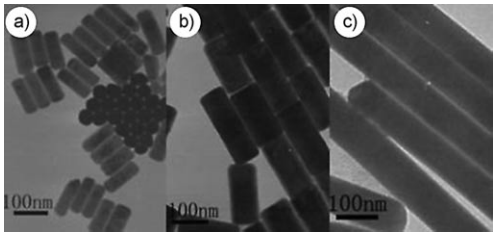

Figure 1. TEM images of the results from LSS syntheses with Ba^{2+} concentrations of a) $0.1000\,mol\,L^{-1}$, b) $0.0750\,mol\,L^{-1}$, c) $0.0375\,mol\,L^{-1}$.

$0.0375\,mol\,L^{-1}$ (Figure 1c). The $BaCl_2$ and HF concentrations were decreased at the same rate as $[Ba^{2+}]$ to keep them in the same ratio, whereas the systematic circumstances of this reaction, such as oleic acid, NaOH, and alcohol, remained unchanged. Vertically stacked nanorods stood upon the surface of a copper grid, with others lying horizontally (Figure 1a). According to this result, a series of deductions were made based on a model that included the specific surface energy of the nanocrystals (including the effect of surfactants), whereas other models in the literature emphasized the solubility of surface molecules.[42]

The chemical growth of nanometer-sized materials inevitably involves the precipitation of a solid phase from solution. A good understanding of the process and parameters controlling the precipitation helps to improve the engineering of the growth of nanoparticles to the desired size. The nucleation process discussed herein, that is, homogeneous nucleation, is expected to occur in the absence of a solid interface by combining solute molecules to produce nuclei. This happens as a result of the driving force of the thermodynamics because the supersaturated solution is not stable in energy. After the nuclei are formed in solution, they grow via molecular addition, which relives the supersaturated conditions. Both the nucleation and growth of the nanomaterials in this work are dominated by thermodynamics.

The fundamental equation of SCT [Eq (1)] may not be accurate enough for a quantitative description of a crystallization process in the nanometer regime, but it should provide us with a starting point.

$$dG = -SdT + Vdp + \gamma d\sigma + \sum_{i=1}^{n} \mu_{Bi} dn_{Bi} \quad (1)$$

In this equation, σ is the surface area of the nanocrystals, γ is the specific surface energy (aka the surface tension), B represents of a certain component, n_B is the molar quantity of this component, μ_B is the chemical potential of each component, T is the absolute temperature, p is pressure, V is the volume of the materials, and S is the entropy of the system. A series of solvothermal syntheses were performed at a fixed temperature, such as 160 °C, for Ba_2F_3Cl nanorods and nanowires. Thus, T was constant and $dT=0$. Moreover, the total volume of each autoclave was considered to be approximately the same and so was the solvent volume. Therefore, the value of p was nearly unchanged and thus $dp=0$. Under conditions of high adsorbate coverage (ligands/surfactant (lig/surf)), it was shown that γ was dominated by the chemical potential of the adsorbate (μ_{ads}).[43]

$$\gamma \approx \gamma_0 - (\mu_{ads} - \mu'_{ads})\Gamma_{max} \quad (2)$$

γ_0 refers to the specific surface energy of pristine interface, μ'_{ads} is defined as the value of μ_{ads} when $\gamma=\gamma_0$, and Γ_{max} is the saturated surface adsorbate density. A basic assumption is that the entire surface of the nanocrystals is saturated by ligands or surfactants. The whole system had in all likelihood reached equilibrium after aging for 24 h. The chemical potential of the surface of nanocrystals ($\mu_{ads(surf)}$) is equal to that of the solution (μ_{sol}). The chemical potential of the adsorbate can be expressed as

$$\mu_{ads(surf)} = \mu_{sol} = \mu_0^{\ominus} + RT\ln a_{lig/surf} + \int_{p^{\ominus}}^{p} V_m^{\infty} dp \quad (3)$$

The solvent activity ($a_{lig/surf}$) is attributed to the concentration of oleic acid, and it is a constant because the concentration of oleic acid is unaltered. The abundance of oleic acid leads to a tremendous absolute value of $a_{lig/surf}$. In principle, if $a_{lig/surf}$ is large enough, a value of $\gamma<0$ can be achieved. Because of the invariability of the concentration of oleic acid, μ_{sol}, $\mu_{ads(surf)}$, and γ are all constants. In other words, the effect of oleic acid combined with the nanocrystals' surface is so vigorous as to expand the SSA of nanocrystals. This increase in surface area is likely to stabilize the system. The impetus of this progress accounts for $\gamma<0$, which arises from a sufficiently high concentration of oleic acid on the surface of the nanocrystals. If we integrate Equation (1), we obtain

$$\Delta G = \gamma\Delta\sigma + \int_{i}^{f} \sum_{i=1}^{n} \mu_{Bi} \mathrm{d}n_{Bi} \quad (4)$$

Here, we assume that the process of subjoining raw materials is reversible, and thereby consider that $\Delta G = 0$. Therefore,

$$-\gamma\Delta\sigma = \int_{i}^{f} \sum_{i=1}^{n} \mu_{Bi} \mathrm{d}n_{Bi} \quad (5)$$

Because $\gamma < 0$, we can assume that $-\gamma > 0$; μ is dependent on the activity of ions in solution, and the chemical potential is expressed in Equation (6) (p is constant, as discussed above).

$$\mu_B = \mu_{B0}^{\ominus} + RT\ln a_B + \int_{p^{\ominus}}^{p} V_{Bm}^{\infty} \mathrm{d}p = \mu_{B0}^{\ominus} + RT\ln a_B \quad (6)$$

Based on the ionic strength definition and the Davies equation, we can apparently obtain $\mathrm{d}n_B > 0$, and therefore, $-\gamma\Delta\sigma > 0$. Moreover, assuming that Equation (7) is correct, μ_B is linear with $\ln c_{Bi}$ (b_B is a constant, c_B is the concentration of compound B).

$$\mu_B = k_B \ln c_B - b_B \quad (7)$$

If μ_{Bi} and n_{Bi} are replaced with c_{Bi} after integration, then Equation (8) is obtained.

$$-\gamma\Delta\sigma = \sum k_{Bi}\Delta[c_{Bi}(\ln c_{Bi} - 1)] \quad (8)$$

From Equation (8), we can conclude that the increase in the concentration of raw materials results in expansion of the nanocrystals' surface area. Therefore, we can draw a tentative conclusion that the addition of raw materials should lead to a larger SSA as long as all the raw materials are increased at the same rate. The details of this deduction can be found in the Supporting Information.

To elucidate this mechanism of nanocrystals growth, we needed more convincing evidence to testify that this growth process is actually under thermodynamic control and not kinetic control. The system was, if anything, kinetically trapped. To prove this, we designed several syntheses that lasted for different periods, and as expected, almost the same result was achieved after ripening for 12, 18, 24, and 48 h, and even after 7 days. Moreover, the Gibbs–Duhem equation [Eq (9)] should be obeyed, that is, when T and p are constant,

$$\sum_{i=1}^{n} n_{Bi} \mathrm{d}\mu_{Bi} = 0 \quad (9)$$

In addition, all the other reactant concentrations needed to change simultaneously with $[Ba^{2+}]$ and to remain at a constant ratio to $[Ba^{2+}]$ to simplify thermodynamic deduction. The experiment phenomena were explained by this SCT mechanism, more evidence should be obtained to confirm this mechanism.

A range of experiments were performed on the Ba_2F_3Cl nanorod and nanowire systems. This was intended to help understand the growth processes that relate to the formation of size-controlled nanocrystals, thus no size sorting was performed for any of the samples used for the measurements discussed below. Transmission electron microscopy (TEM) and scanning electron microscopy (SEM) images are shown in Figure 2a–l. If the concentration of all the reactants was relatively high, relatively small nanorods were achieved. Some of them, especially those nanorods with a low length-to-width ratio, assembled perpendicular to the substrate, which we observed in both the TEM and SEM results (Figure 2a–f; see the Supporting Information, Figures S1 and S2). If the concentration of all reactants was decreased to a certain value, Ba_2F_3Cl nanowires were produced (Figure 2i–l). Details of the initial concentrations used are shown in Table 1. Herein, we speculated that during the growth of Ba_2F_3Cl nanorods and nanowires, the surfactant (oleic acid molecules) bound to all the surfaces of the nanocrystals. The high-resolution (HR) TEM image (Figure 3b) clearly shows that the growth is along ⟨541⟩ direction. In addition, the (410) and (541) surfaces dominate both the HRTEM image

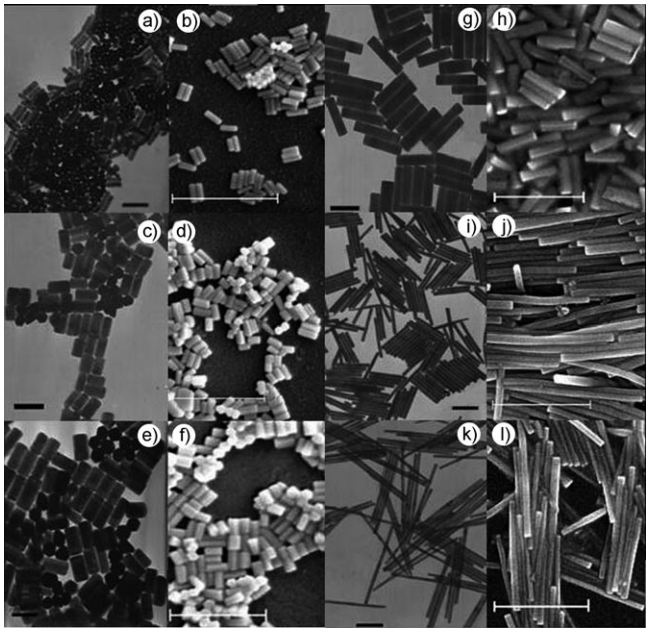

Figure 2. Representative TEM images (a, c, e, g, i, k) and SEM images (b, d, f, h, j, i) of Ba_2F_3Cl nanorods synthesized with the following initial concentrations of Ba^{2+}: a,b) 0.100 mol L^{-1}, c,d) 0.0875 mol L^{-1}, e,f) 0.075 mol L^{-1}, g,h) 0.050 mol L^{-1}, i,j) 0.0375 mol L^{-1}, and k,l) 0.025 mol L^{-1}. All other reactant concentrations were kept at a constant ratio to $[Ba^{2+}]$. The scale bars are 200 nm in images a), c), e), and g); 500 nm in images i) and k); and 1 μm in all the SEM images.

Table 1. The average size and δ of Ba_2F_3Cl nanorods and nanowires.[a]

Initial $[Ba^{2+}]$ [mol L^{-1}]	Average width [nm]	Average length [nm]	Average δ [%]
0.1000	≈40	≈120	14.7
0.0875	≈60	≈150	10.1
0.0750	≈80	≈180	7.7
0.0500	≈80	≈300	7.1
0.0375	≈80	≈1000	6.5
0.0250	≈80	≈1500	6.5

[a] All products were synthesized with all other reactant concentrations kept at a constant ratio to $[Ba^{2+}]$.

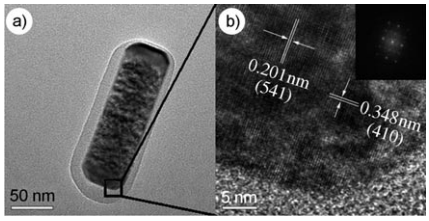

Figure 3. a) A typical HRTEM image of nanorods and b) a HRTEM image and electron diffraction pattern of the inside of a Ba_2F_3Cl nanorod.

(Figure 3b) and the powder XRD pattern (Figure 4). Figure 3a shows that the Ba_2F_3Cl nanorods have slightly decomposed under the electron beam of the HRTEM instrument.

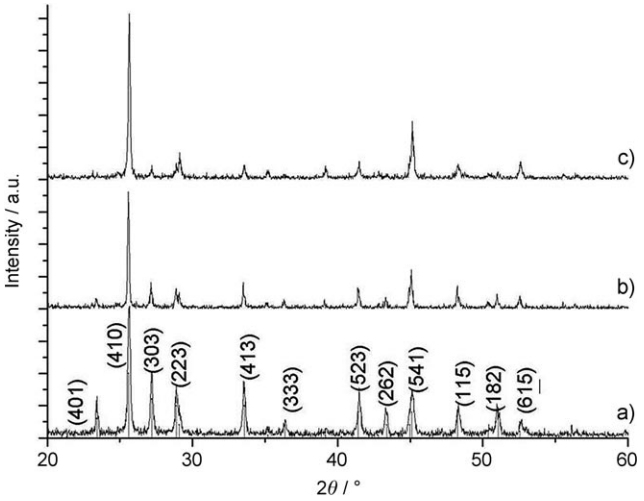

Figure 4. Powder XRD patterns for a) Ba_2F_3Cl nanorods corresponding to the sample in Figure 2a (the samples in Figure 2c, e, and g have a similar XRD pattern), b) Ba_2F_3Cl nanowires corresponding to the sample in Figure 2i, and c) Ba_2F_3Cl nanowires corresponding to the sample in Figure 2k (JCPDS card No. 07-0029).

All the as-synthesized nanocrystals were characterized by powder XRD methods; for the sake of succinctness, however, only three XRD patterns for the nanocrystals are shown here (Figure 4a, b, and c). When the initial value of $[Ba^{2+}]$ decreased from 0.1125 to 0.0500 mol L^{-1}, the powder XRD patterns of the product were similar to Figure 4a, and their TEM images are depicted in Figure 2a, c, e, and g. Figure 4b and c shows powder XRD patterns of the nanocrystals shown in Figure 2i and k, respectively, in which the initial values of $[Ba^{2+}]$ are 0.0375 mol L^{-1} and 0.0250 mol L^{-1}. We can easily see that they are all pure-phase Ba_2F_3Cl (JCPDS card No. 07-0029), and that the (541) and (410) diffraction peaks become more and more dominant in the powder XRD patterns from Figure 4a to c. The nanocrystals mainly showed (541) and (410) profiles, which are shown in the HRTEM image in Figure 3b. A low initial concentration leads to larger nanocrystals, that is, the percentage of the surface/area ratio increases. Thus, (541) and (410) become dominant, which is reflected in the powder XRD results (Figure 4a, b, and c). Intense diffraction peaks suggest that (541) and (410) were more exposed under low initial concentrations than under higher initial concentrations. For these nanorods and nanowires, the number of surface atoms and the total number of atoms should be proportional to the surface area and the volume, respectively. We define δ as follows:

$$\delta = \frac{k_1(2\pi(\frac{d}{2})^2 + 2\pi(\frac{d}{2})l)}{k_2\pi(\frac{d}{2})^2 l} = 2k_3(\frac{1}{l} + \frac{2}{d}) \qquad (10)$$

in which k_1, k_2, and k_3 are all proportional constants, d is the diameter of the nanorods or nanowires, and l represents the length of the nanocrystals.[21] The derivation of Equation (10) is shown in the Supporting Information.

After simple calculation, Table 1 gives the average size and surface-area ratio of each type of product. Moreover, the curve of Figure 5, which is based on the data in Table 1, shows a trend in which a higher initial concentration results in a higher average atom ratio, that is, the nanocrystals are smaller, which means that the surface area of nanocrystals is larger for the same amount of nanocrystals. This result commendably validates the SCT mechanism discussed above; as

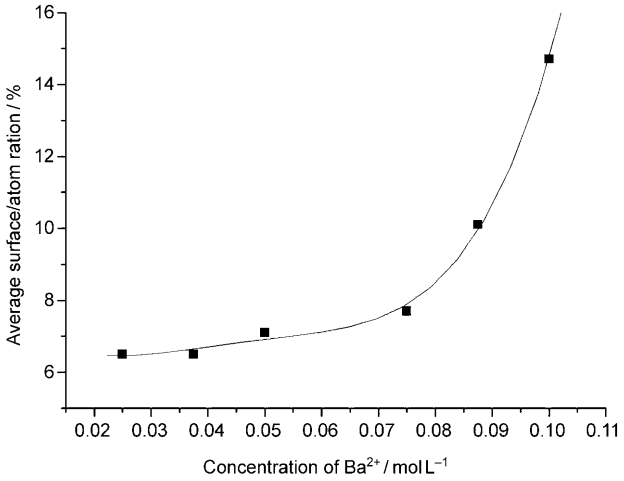

Figure 5. Concentration dependence of the δ value of Ba_2F_3Cl nanocrystals, (assuming a rod or wire shape). This curve shows the trend that the value of δ is higher if the initial concentration is greater.

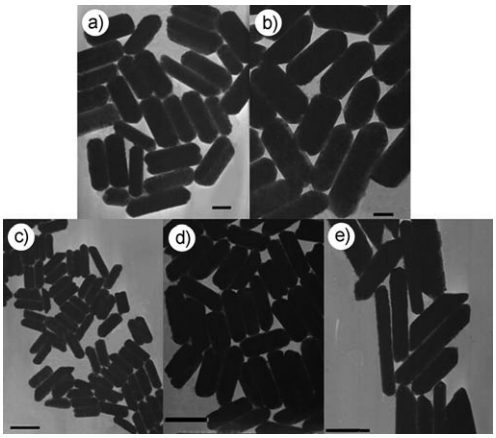

Figure 6. TEM images of orthorhombic BaF_2 nanorods synthesized with initial concentrations of Ba^{2+} of a) 0.0750 mol L^{-1}, b) 0.0625 mol L^{-1}, c) 0.0500 mol L^{-1}, d) 0.0375 mol L^{-1}, and e) 0.0250 mol L^{-1}. All other reactants were kept at a constant ratio to $[Ba^{2+}]$. The scale bars are 100 nm in a) and b) and 500 nm in c), d), and e).

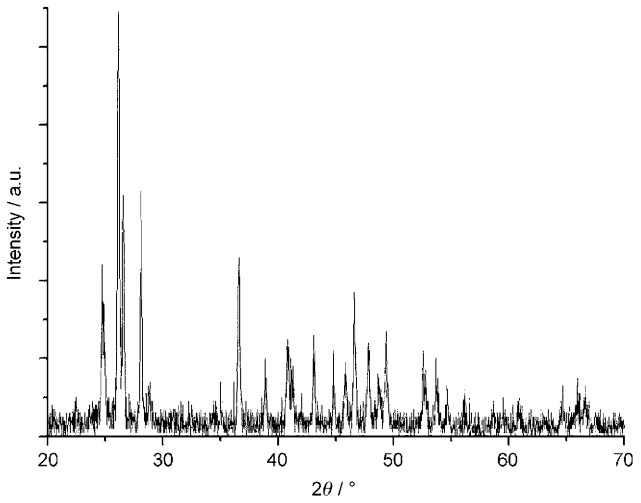

Figure 7. Powder XRD pattern of orthorhombic BaF_2 nanorods. (JCPDS card No. 34-0200).

mentioned, this mechanism is applicable in a Ba_2F_3Cl preparation system. We also scrutinized other, similar systems, and discovered that the synthesis of BaF_2 nanocrystals also obeys the rule that a high initial concentration gives a high average atom ratio.

Orthorhombic BaF_2 was also one of our targets for investigation. To the best of our knowledge, orthorhombic BaF_2 nanorods have rarely been reported before. Herein, different sizes of orthorhombic BaF_2 nanorods have been prepared by using an LSS strategy (Figure 6). Orthorhombic BaF_2 nanorods were gained when the initial values of $[Ba^{2+}]$ were 0.0750 mol L^{-1}, 0.0625 mol L^{-1}, 0.0500 mol L^{-1}, 0.0375 mol L^{-1}, and 0.0250 mol L^{-1} (see Figure 6a, b, c, d, and e, respectively) with all other reactants being maintained at a constant ratio to $[Ba^{2+}]$. Their powder XRD patterns are all almost identical (Figure 7), and show that we have obtained pure-phase orthorhombic BaF_2 nanorods. (JCPDS card No. 34-0200) The average size and surface/atom ratio of each kind of orthorhombic BaF_2 nanorods are listed in Table 2, and the calculation results from Equation (10) were given by using a graph (Figure 8). The curve of the graph suggests the trend is the same as described above, that is, the surface atom ratio increases as the initial concentration increases, as predicted herein based on the SCT mechanism.

Table 2. The average size and δ of orthorhombic BaF_2 nanorods.[a]

Initial $[Ba^{2+}]$ [mol L^{-1}]	Average width [nm]	Average length [nm]	Average δ [%]
0.0750	≈100	≈250	1.9
0.0625	≈150	≈350	1.3
0.0500	≈150	≈500	1.2
0.0375	≈200	≈650	0.93
0.0250	≈200	≈800	0.91

[a] All products were synthesized with all other reactant concentrations kept at a constant ratio to $[Ba^{2+}]$.

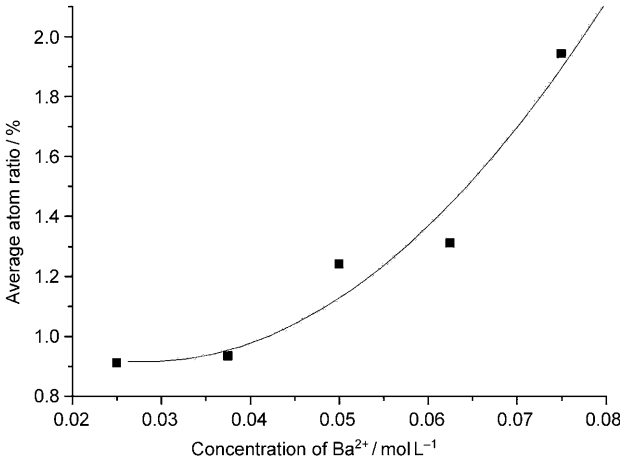

Figure 8. Concentration dependence of the δ value of orthorhombic BaF_2 nanorods (assuming a rod shape). This curve shows the trend that as the initial concentration increases, so does the average atom ratio, which implies that the nanocrystals are larger, just as for Ba_2F_3Cl nanocrystals.

Conclusion

In a nutshell, an SCT mechanism was devised to explain the experiment phenomena. Several systems, such as Ba_2F_3Cl nanorods and nanowires and orthorhombic BaF_2 nanorods, were investigated to support this SCT mechanism. To the best of our knowledge, all these systems are only scarcely reported in the literature. The conclusion that higher concentration accounts for higher surface atom ratio (i.e., smaller nanocrystals) could introduce a convenient way to control the size of nanocrystals. This shape- and size-controlling condition is not only simple, but can also be executed easily; the initial concentration of reactants was the only parameter we changed in this work. The successful explanation of these processes by using an SCT mechanism gave us the confidence to use fundamental formulae and equations from

physical chemistry to understand the nucleation and growth of nanocrystals. It is highly possible that this SCT mechanism can be used to guide the preparation of nanocrystals in the near future. However, it should be noted that we chose only two systems to validate this mechanism herein, and only one type of solvent and surfactant was considered. More experiments examining other systems are required to fully assess this conclusion.

Experimental Section

Materials: All chemicals were of analytical grade and were used as received without further purification. Deionized water was used throughout. $BaCl_2$, $Ba(NO_3)_2$, HF (40 wt%), oleic acid, NaOH, and alcohol were all supplied by the Beijing Chemical Reagent Company.

Synthesis of the nanocrystals: In a typical preparation of nanorods, oleic acid (20 mL), NaOH (1.8 g), alcohol (10 mL), and barium salt (4 mmol) in water ($\approx$7 mL) were mixed, and an even solution was obtained by vigorous stirring at RT for about 10 min. A white amorphous precipitate appeared immediately after the dropwise addition of an aqueous solution of HF (3.0 mL, 5 wt%) to this emulsion. After vigorous stirring at RT for about another 10 min, the mixture was transferred into a 50 mL autoclave, sealed, and heated at 160 °C for 24 h. Then the system was allowed to cool down to RT and the product deposited at the bottom of the vessel.

For the synthesis of orthorhombic BaF_2, $Ba(NO_3)_2$ was used as the precursor instead of $BaCl_2$, and the quantity of HF used was changed appropriately. The autoclave was sealed and heated at 160 °C for 6 h. In fact, these nanocrystals were prepared by adapting our group's previously reported LSS synthetic strategy. Detailed initial concentrations of the reactants have been summarized herein in Tables 1 and 2.

Powder X-ray Diffraction: The crystallinity and phase purity of the products were examined with XRD by using a Bruker D8-advance X-ray diffractometer with $Cu_{K\alpha}$ radiation ($\lambda = 1.5418$ Å), with an operating voltage of 40 kV and a current of 40 mA.

Transmission electron microscopy: The size and morphology of the products were observed by using a JEOL JEM-1200EX transmission electron microscope equipped with a tungsten filament at an accelerating voltage of 100–120 kV. Samples were prepared by placing a drop of a dilute dispersion of nanocrystals in cyclohexane on the surface of a copper grid. HRTEM images were obtained on a JEOL JEM-2010F transmission electron microscope.

Scanning electron microscopy: The size and morphology of the nanorods were examined by using a JEOL JSM-6301F scanning electron microscope operating at 20 kV.

Acknowledgements

This work was supported by the NSFC (No. 90606006), the State Key Project of Fundamental Research for Nanoscience and Nanotechnology (No. 2006CB932300) and the Key Grant Project of Chinese Ministry of Education (No. 306020).

[1] C. B. Murray, D. J. Norris, M. G. Bawendi, *J. Am. Chem. Soc.* **1993**, *115*, 8706–8715.
[2] C. B. Murray, C. R. Kagan, M. G. Bawendi, *Annu. Rev. Mater. Sci.* **2000**, *30*, 545–610.
[3] C. M. Lieber, *Solid State Commun.* **1998**, *107*, 607–616.
[4] V. F. Puntes, K. M. Krishnan, A. P. Alivisatos, *Science* **2001**, *291*, 2115–2117.
[5] E. V. Shevchenko, D. V. Talapin, N. A. Kotov, S. O'Brien, C. B. Murray, *Nature* **2006**, *439*, 55–59.
[6] C. B. Murray, C. R. Kagan, M. G. Bawendi, *Science* **1995**, *270*, 1335–1338.
[7] C. Burda, X. Chen, R. Narayanan, M. A. El-Sayed, *Chem. Rev.* **2005**, *105*, 1025–1102.
[8] A. P. Alivisatos, *Science* **1996**, *271*, 933–937.
[9] J. B. Jackson, N. J. Halas, *J. Phys. Chem. B* **2001**, *105*, 2743–2746.
[10] M. A. El-Sayed, *Acc. Chem. Res.* **2001**, *34*, 257–264.
[11] M. A. El-Sayed, *Acc. Chem. Res.* **2004**, *37*, 326–333.
[12] H. Lee, S. E. Habas, S. Kweskin, D. Butcher, G. A. Somorjai, P. D. Yang, *Angew. Chem.* **2006**, *118*, 7988–7992; *Angew. Chem. Int. Ed.* **2006**, *45*, 7824–7828.
[13] L. Z. Zhang, Z. H. Ai, F. L. Jia, L. Liu, X. L. Hu, J. C. Yu, *Chem. Eur. J.* **2006**, *12*, 4185–4190.
[14] X. L. Li, Q. Peng, J. X. Yi, X. Wang, Y. D. Li, *Chem. Eur. J.* **2006**, *12*, 2383–2391.
[15] P. Ebert, *Surfactant Sci. Ser.* **1999**, *33*, 121–303.
[16] A. P. Alivisatos, *J. Phys. Chem.* **1996**, *100*, 13226–13239.
[17] M. Nirmal, L. Brus, *Acc. Chem. Res.* **1999**, *32*, 407–414.
[18] H. Deng, J. W. Wang, Q. Peng, X. Wang, Y. D. Li, *Chem. Eur. J.* **2005**, *11*, 6519–6524.
[19] Z. Y. Huo, C. Chen, D. Chu, H. H. Li, Y. D. Li, *Chem. Eur. J.* **2007**, *13*, 7708–7714.
[20] X. G. Peng, L. Manna, W. D. Yang, *Nature* **2000**, *404*, 59–61.
[21] Z. A. Peng, X. G. Peng, *J. Am. Chem. Soc.* **2002**, *124*, 3343–3353.
[22] N. Pradhan, D. Reifsnyder, R. Xie, J. Aldana, X. Peng, *J. Am. Chem. Soc.* **2007**, *129*, 9500–9509.
[23] Y. G. Sun, Y. N. Xia, *Science* **2002**, *298*, 2176–2179.
[24] J. Park, J. Joo, S. G. Kwon, Y. Jang, T. Hyeon, *Angew. Chem.* **2007**, *119*, 4714–4745; *Angew. Chem. Int. Ed.* **2007**, *46*, 4630–4660.
[25] Y. W. Jun, J. W. Seo, S. J. Oh, J. Cheon, *Coord. Chem. Rev.* **2005**, *249*, 1766–1775.
[26] T. S. Ahmadi, Z. L. Wang, T. C. Green, A. Henglein, M. A. El-Sayed, *Science* **1996**, *272*, 1924–1926.
[27] K. T. Yong, Y. Sahoo, K. R. Choudhury, M. T. Swihart, J. R. Minter, P. N. Prasad, *Nano Lett.* **2006**, *6*, 709–714.
[28] X. Wang, J. Zhuang, Q. Peng, Y. D. Li, *Nature* **2005**, *437*, 121–124.
[29] X. Y. Kong, Y. Ding, R. Yang, Z. L. Wang, *Science* **2004**, *303*, 1348–1351.
[30] N. Tian, Z. Y. Zhou, S. G. Sun, Y. Ding, Z. L. Wang, *Science* **2007**, *316*, 732–735.
[31] S. F. Chen, S. H. Yu, B. Yu, L. Ren, W. T. Yao, H. Colfen, *Chem. Eur. J.* **2004**, *10*, 3050–3058.
[32] M. Kobayashi, *Solid State Ionics* **2004**, *174*, 57–66.
[33] B. Liu, Y. H. Chen, C. S. Shi, H. G. Tang, Y. Tao, *J. Lumin.* **2003**, *101*, 155–159.
[34] C. M. Bender, J. M. Burlitch, D. Barber, C. Pollock, *Chem. Mater.* **2000**, *12*, 1969–1976.
[35] M. H. Cao, C. W. Hu, E. B. Wang, *J. Am. Chem. Soc.* **2003**, *125*, 11196–11197.
[36] R. N. Hua, C. Y. Zang, C. Sha, D. M. Xie, C. S. Shi, *Nanotechnology* **2003**, *14*, 588–591.
[37] B. Liu, Y. H. Chen, C. S. Shi, H. G. Tang, Y. Tao, *J. Lumin.* **2003**, *101*, 155–159.
[38] P. Gao, Y Xie, Z. Li, *Euro. J. Inorg. Chem.* **2006**, *16*, 3261–3265.
[39] G. H. De, W. P. Qin, J. Zhang, J. H. Zhang, Y. Wang, C. Y. Cao, Y. Cui, *J. Solid State Chem.* **2006**, *179*, 955–958.
[40] Z. B. Zhuang, Q. Peng, J. Zhuang, X. Wang, Y. D. Li, *Chem. Eur. J.* **2005**, *11*, 211–217.
[41] X. Liang, X. Wang, J. Zhuang, Y. T. Chen, D. S. Wang, Y. D. Li, *Adv. Func. Mater.* **2006**, *16*, 1805–1813.
[42] I. L. Mladenovic, W. K. Kegel, P. Bomans, P. M. Frederik, *J. Phys. Chem. B* **2003**, *107*, 5717–5722.
[43] Z. Lin, B. Gilbert, Q. L. Liu, G. Q. Ren, F. Huang, *J. Am. Chem. Soc.* **2006**, *128*, 6126–6131.

Received: February 28, 2008
Revised: June 20, 2008
Published online: September 9, 2008

